Effects of Surfactant on the Motion of Large Bubbles in a Capillary Tube

by

Gökalp Gürsel

A Thesis Submitted to the
Graduate School of Engineering
in Partial Fulfillment of the Requirements for
the Degree of

Master of Science
in
Mechanical Engineering

Koc University
August 2011

Koc University

Graduate School of Sciences and Engineering

This is to certify that I have examined this copy of a master's thesis by

Gökalp Gürsel

and have found that it is complete and satisfactory in all respects,
and that any and all revisions required by the final
examining committee have been made.

Committee Members:

_____

Assoc. Prof. Metin Muradoğlu

_____

Assoc. Prof. Ali Koşar

_____

Asst. Prof. Mehmet Şahin

Date: _____

ABSTRACT

The finite-difference/front-tracking method is used to study the motion and deformation of a large bubble moving through a capillary tube in the presence of both insoluble and soluble surfactant. Effects of surfactant on the liquid film thickness between the bubble and the tube wall are the main subject of this study. The numerical method is designed to solve the evolution equations of the interfacial and bulk surfactant concentrations coupled with the incompressible Navier-Stokes equations. A non-linear equation of state is used to relate interfacial surface tension to interfacial surfactant concentration. First, computations are performed to study the film thickness for the clean bubble case and results are compared with the semi-analytical Taylor's Law [1]. It is found that our results are in a good agreement with the Taylor's Law [1]. Following, the method is used to investigate the effects of insoluble and soluble surfactants on the film thickness for a wide range of governing non-dimensional numbers. It is found that both the insoluble and soluble surfactants have a thickening effect on the liquid film, which compares qualitatively well with both the experimental results of Krechetnikov and Homsy [2] and analytical predictions of Daripa and Pasa [3]. Further computations are performed to examine the effects of non-dimensional numbers in the insoluble and soluble surfactant cases and it is found that elasticity, Damkohler and Peclet numbers have significant influence on the film thickness.

ÖZET

Büyük gaz kabarcıklarının kılcal borulardaki çözünebilir ve çözünemez yüzey aktif maddelerin varlığında hareket ve şekil değişimlerini incelemek için, sonlu-farkla/arayüz-izleme metodu kullanıldı. Bu çalışmadaki en önemli konu yüzey aktif maddelerin, kabarcık ve kılcal boru arasında oluşan ince sıvı tabakası üzerindeki etkilerinin incelenmesidir. Sıkıştırılamaz akış denklemleri, arayüde ve gaz kabarcığının bulunduğu çevre ortamda yüzey aktif madde taşınım denklemleri ile bağlı şekilde çözüldü. Yüzey gerilimini yüzey aktif maddenin fonksiyonu olarak tanımlamak için, doğrusal olmayan bir hal denklemi kullanıldı. İlk olarak temiz kabarcığın yüzeyi ile kılcal boru arasında oluşan ince tabaka incelendi ve küçük capillary sayılarında yarı analitik Taylor Kanunu [1] ile karşılaştırıldı. Sonuçların Taylor Kanunu [1] ile uyumlu olduğu gözlemlendi. Bu incelemeyi takiben, çözünebilir ve çözünemez yüzey aktif maddelerin çeşitli boyutsuz sayılarda ince tabaka üzerindeki etkisi incelendi. İncelemelerin sonucu olarak, hem çözünebilir hem de çözünemez yüzey aktif maddelerin ince tabakanın kalınlığını arttırdığı görüldü ki bu davranış hem Krechetnikov ve Homsy'nin [2] deneysel çalışmaları hem de Daripa ve Pasa'nın [3] analitik çalışması ile uyumludur. Bu aşamadan sonra boyutsuz sayıların hem çözünebilir hem de çözünemez yüzey aktif maddeli durumlarda ki etkisi araştırıldı ve elastisite, Damkohler ve Peclet sayılarının ince sıvı tabaka kalınlığını önemli ölçüde etkilediği görüldü.

ACKNOWLEDGEMENTS

First of all, I would like to express my sincere thanks to my advisor, Associate Prof. Metin Muradoğlu for his very friendly and knowledgeable guidance during this study and endless support at every phase of my gradute study.

I am grateful to members of my thesis committee (Metin Muradoğlu, Ali Koşar and Mehmet Şahin) for critical reading of this thesis and for their valuable comments.

I would like to thank to my research group friend Ufuk Olgaç for his friendly help at the second year of my graduate study.

Many thanks are due to my grad student friends whose friendship have made the years in Koç University a memorable time in my life.

Last but not least, I would like to thank my parents Saadet and Haluk and my dear wife Iris who have always loved and supported me.

TABLE OF CONTENTS

LIST OF FIGURES

NOMENCLATURE

u	velocity
p	pressure
ρ_o	density of the ambient fluid
ρ_b	density of the bubble
μ_o	viscosity of the ambient fluid
μ_b	viscosity of the bubble
t	physical time
t^*	non-dimensional time
s	arc length
σ	surface tension
κ	curvature
x	location of a front point
x_f	location of the front
I	indicator function
M_s	total mass of surfactant
A	surface area
R	ideal gas constant
T	absolute temperature
δ	Delta function
R_c	channel radius
L	channel length
Γ	surfactant concentration at the interface
Γ_{eq}	equivalent surfactant concentration at the interface
Γ_∞	maximum surfactant concentration at the interface

D_s	surface diffusion coefficient
D_c	molecular diffusion coefficient
D_{co}	bulk diffusion coefficient
C	bulk surfactant concentration
C_∞	maximum bulk surfactant concentration
C_s	surfactant concentration in fluid immediately adjacent to the interface
Ca_{eff}	effective Capillary number
σ_s	surface tension of a clean interface
σ_{eff}	equivalent surface tension
σ_{ave}	average surface tension
L	length scale
U	velocity scale
T	time scale
Re	Reynolds number
Ca	Capillary number
Pe_c	Peclet number based on bulk surfactant diffusivity
Pe_s	Peclet number based on interface surfactant diffusivity
Da	Damkohler number
k	dimensionless adsorption depth
Bi	Biot number
k_a	adsorption coefficient
k_b	desorption coefficient
βs	Elasticity number

Chapter 1

INTRODUCTION

The displacement of liquid by a gas bubble moving through a capillary tube is a model widely used to analyze a variety of complex multiphase flow problems. It thus has received considerable attention since the pioneering work of Bretherton [4], who investigated the motion of long bubbles in capillary tubes. Bretherton problem has been used as a model in many areas such as flow in porous media [5], water or foam flooding in enhanced oil recovery [6] and biomechanics [5]. To develop a simple model for porous media, bundle of capillary tube model is used [6]. As a model for water or foam flooding in enhanced oil recovery, displacement flow in capillary tubes is used [6]. Regarding biomechanics, one interesting example is the re-opening of collapsed pulmonary airways. The simplest model of this phenomenon is the motion of semi-infinite bubble in a capillary tube initially filled with a viscous liquid.

An important issue in multiphase systems is the role played by surface-active agents (surfactants) that are present either as impurities, which are difficult to remove from the system, or as additives to manipulate the interfacial dynamics. It is well-known that the

surfactants largely affect the dynamic behavior of deforming interfaces. The presence of surfactants in a fluid mixture can critically alter the motion and deformation of bubbles moving through a continuous liquid phase [7,8]. In particular, surfactants play a critical role in pulmonary re-opening [9]. Surfactant molecules attach to the interface and form a buffer zone between the gas and liquid phases. They interact with the cohesive forces between the liquid molecules and reduce the surface tension and stabilize the interface [10]. In a static system, interfacial surfactant concentration has a saturation value, for which surface tension has its minimum. However, in a dynamic system, such as alveoli, interfacial surfactant concentration value can exceed the maximum packing value under dynamic conditions due to surface compression, which results in significant reduction in surface tension [11-13]. When surfactants are present, surface tension changes with the interfacial surfactant concentration and Marangoni stresses may develop when the surfactant concentration is not uniform on the interface.

Pulmonary surfactant is required for normal lung functioning. Pulmonary surfactant is absorbed on the thin liquid film that covers the surface of the airways and the alveoli and reduces the surface tension on the liquid-gas interface and the work required to expand the lung at each breath. Due to surfactant-deficiency, surface tension on the air-liquid interface might get elevated and the airways might get closed since the flexible structure of the tubes causes unstable support for the airways. Airway closure may also occur due to Rayleigh instability of the liquid lining of the tubes [14]. In both ways the airway is closed as a liquid

plug forms preventing the passage of gas. Airway closure may occur in normal lungs when the lung reaches very low volumes [15]. Liquid plugs could also occur in case of diseases such as respiratory distress syndrome (RDS), asthma, pulmonary edema and emphysema. The primary way to reopen the airway is through inhalation [10]. During inhalation the liquid plug is forced to flow until it resides on the airway walls and eventually ruptures allowing gas exchange [10]. Healthy adults are able to reopen the airways in this way, however people with respiratory diseases cannot produce enough pressure to reopen their airways [11]. A primary deficiency of surfactant in prematurely born neonates prevents the normal transition from a fluid filled to an aerated lung at birth known as RDS. In RDS, the airways are closed due to elevated surface tension on the air-liquid interface. Surfactant replacement therapy (SRT) is used for premature neonates for the treatment of RDS, in which a liquid plug with exogenous surfactant is instilled into the airways.

A thin film of liquid is deposited on the walls when displacement of a large bubble in a viscous liquid occurs inside the capillary tube. The motion of a semi-infinite bubble in a capillary tube was originally studied by Fairbrother & Stubbs [16], Bretherton [4], and Taylor [17]. It has been later studied by many and findings have been reported in a number of papers [18-21]. In the absence of surfactants, studies show that the thickness of the liquid film left behind by the creeping motion ($Re<<1$) of a semi-infinite bubble depends solely on the Capillary number defined as $Ca = \mu U_b/\sigma$, where U_b is the bubble velocity, μ is the viscosity of the liquid and σ is the surface tension on the air-liquid interface [1]. The

film thickness depends on both the Capillary number and Reynolds number ($Re = \rho UR/\mu$) in large airways due to the importance of inertial forces ($Re>>1$), where ρ, U and R are the density of the liquid, the flow velocity and the channel radius, respectively.

More recently the influence of surfactants on the displacement of a confined gas-liquid interface has been analyzed analytically [3-4, 19, 22-23], experimentally [2, 17, 20-21] and numerically [11, 24-25]. The numerical works of Wassmuth et al. [24], Severino et al. [25], Ghadiali and Gaver [11] deal with the effects of soluble and insoluble surfactants. Wassmuth et al. [24] numerically investigated the motion of the bubble-liquid interface between parallel plates. Severino et al. [25] performed similar studies and aimed to identify the film thickness as a function of relevant dimensionless numbers in dip coating systems. Ghadiali and Gaver [11] reported numerical results for a semi-infinite bubble moving in a capillary tube filled with a surfactant solution. They found that depending upon the range of dimensionless parameters, i.e., Peclet number, and adsorption and desorption Stanton numbers, either film thickening or film thinning responses are possible. It was demonstrated that there is a non-monotonic behavior between Peclet number and liquid film thickness.

Ratulowski and Chang [18] carried out asymptotic analysis in the case of very slow motions and traces of surfactant to obtain solutions for both the hydrodynamics and mass transfer problems. They found, for the first time, that surfactants increase the film thickness by a maximum factor of $4^{2/3}$ compared with the surfactant-free case for infinitely long

bubbles. Park [23] analytically investigated the effects of surfactants on the motion of a finite bubble in the small capillary number regime. They also performed an asymptotic analysis to relate interfacial surfactant concentration to adsorption-desorption kinetics. They also focused on the case, in which axial diffusion of the surfactant in the bulk is slower than adsorption and bulk convection, and adsorption is faster than surface convection. This flow situation was described as the convective equilibrium model. It was shown that under these conditions Marangoni effects could increase the thickness of the liquid film laid under the bubble by a maximum factor of $4^{2/3}$ compared to the surfactant-free case. Stebe and Barthes-Biesel [19] suggested that the surfactant exchange between liquid phase and the interface is controlled by the desorption kinetics. Their analysis aims at revealing potential effects of surfactants on the liquid film thickness. They found that Marangoni stresses that result from hindered sorptive exchange caused thicker wetting layers. Recently, Daripa and Pasa [3] reported analytical results on the effects of surfactants on the motion of long bubbles in horizontal capillary tubes. They showed that the liquid film between the bubble and the wall was thicker in a surfactant solution compared to that in a clean liquid.

Krechetnikov and Homsy [2] reported experimental results on the surfactant effects on the Landau-Levich problem. This problem is essentially the same as Bretherton's problem as they both relate film thickness to Capillary number. Landau-Levich problem investigates the coating of a flat plate as it is withdrawn from a stagnant liquid bath whereas Bretherton

deals with the motion of long bubbles in capillary tubes. The main goal of Krechetnikov and Homsy [2] was to confirm the thinning effect of surfactant, which they previously numerically observed [26]. They suggested that Marangoni effects could lead to film thinning at the sorption-controlled coating regime. Schwartz et al. [21] also reported experimental results on the surfactant effects on the film thickness. They found that for sufficiently small bubbles, the film thicknesses agreed well with the predictions of lubrication theory. For long bubbles, e.g., $R_b > R_c$ on the other hand, they measured a different 'solution curve', which suggests that lubrication theory is not valid. The deviation between the small and large bubbles becomes more pronounced at low speeds. Furthermore, Chen [20] measured the film thickness surrounding a bubble inside a capillary and found that film thickness decreases with decreasing bubble speed.

The aim of this study is to numerically investigate the effects of soluble and insoluble surfactants and various non-dimensional parameters on the motion of long bubbles and the film thickness in a capillary tube. Additionally, a range of non-dimensional parameters is sought, in which the insoluble surfactant assumption is valid. For this purpose, the incompressible Navier–Stokes equations are solved fully coupled with the evolution equations of the interfacial and bulk surfactant concentrations by using a finite-difference/front-tracking method developed by Muradoglu and Tryggvason [27]. A nonlinear equation of state based on the Langmuir adsorption [28] is used to relate the surface tension coefficient to the interfacial surfactant concentration. Unsteady

computations are performed to examine the evolution of interfacial and bulk surfactant concentrations.

The remainder of the thesis is organized as follows: In the next section, the mathematical formulation is presented and the numerical method is briefly reviewed. Problem statement is also presented in Sec.2. The results are presented and discussed in Sec. 3 and the conclusions are presented in Sec. 4. Grid convergence is discussed in the Appendix.

Chapter 2

MATHEMATICAL FORMULATION AND NUMERICAL METHOD

2.1 Mathematical Formulation

In this section flow equations are described in the context of the finite-difference/front-tracking method for axisymmetric problem. The incompressible Navier-Stokes equations are used to represent the fluid motion. Flow equations are solved for entire domain (both inside and outside of the bubble). Following Unverdi and Tryggvason [29], a single set of governing equations can be written for the entire computational domain provided that the jumps in the material properties such as density, viscosity and molecular diffusion coefficient are correctly accounted for and surface tension is included.

In an axisymmetric coordinate system, the Navier-Stokes equations in conservative form are given by

$$\frac{\partial \rho u}{\partial t}+\frac{1}{r}\frac{\partial r\rho u^2}{\partial r}+\frac{\partial \rho uv}{\partial z} = -\frac{\partial p}{\partial r}+\frac{\partial}{\partial r}\left(2\mu\frac{\partial u}{\partial r}\right)+2\mu\frac{\partial}{\partial r}\left(\frac{u}{r}\right)+\frac{\partial}{\partial z}\mu\left(\frac{\partial v}{\partial r}+\frac{\partial u}{\partial z}\right) - \int_A \sigma(\Gamma)\kappa\mathbf{n}\delta(\mathbf{x}-\mathbf{x}_f)d\mathbf{A}\cdot\hat{\mathbf{i}}_r \tag{2.1}$$

$$\frac{\partial \rho v}{\partial t}+\frac{1}{r}\frac{\partial r\rho uv}{\partial r}+\frac{\partial \rho v^2}{\partial z} = -\frac{\partial p}{\partial z}+\frac{\partial}{\partial r}\mu r\left(\frac{\partial v}{\partial r}+\frac{\partial u}{\partial z}\right)+\frac{\partial}{\partial z}\left(2\mu\frac{\partial v}{\partial z}\right)-\int_A \sigma(\Gamma)\kappa\mathbf{n}\delta(\mathbf{x}-\mathbf{x}_f)d\mathbf{A}\cdot\hat{\mathbf{i}}_z$$

where u and v are the velocity components in the radial and axial directions, respectively, and p, ρ and μ are the pressure, and the discontinuous density and viscosity fields, respectively. The last term on the right hand side is a body force that includes the effects of surface tension. In this term σ is the surface tension that is a function of the surfactant concentration Γ at the interface, κ is twice the mean curvature, and $\mathbf{n}=\hat{\mathbf{i}}_r+\hat{\mathbf{i}}_z$ is a unit vector normal to the interface. The surface tension only acts on the interface as indicated by the three dimensional delta function δ, whose arguments $\mathbf{x}$ and $\mathbf{x_f}$ are the point at which the equation is evaluated and the point at the interface, respectively.

The Navier-Stokes equations are supplemented by the incompressibility condition,

$$\frac{1}{r}\frac{\partial ru}{\partial r}+\frac{\partial v}{\partial z}=0. \tag{2.2}$$

We also assume that the material properties remain constant following a fluid particle,

$$\frac{D\rho}{Dt}=0;\ \frac{D\mu}{Dt}=0, \tag{2.3}$$

where D/Dt is the material derivative. The density and viscosity vary continuously across the fluid interface and are given by

$$\rho=\rho_b I(r,z,t)+\rho_o\left(1\text{-}I(r,z,t)\right)$$
$$\mu=\mu_b I(r,z,t)+\mu_o\left(1\text{-}I(r,z,t)\right) \tag{2.4}$$

where the subscripts b and o denote properties of the bubble and the ambient fluids, respectively and I(r,z,t) is the indicator function defined as

$$I(r,z,t)=\begin{cases}1 & \text{in bubble fluid}\\ 0 & \text{in bulk fluid.}\end{cases} \tag{2.5}$$

Concentration of surfactant on the interface Γ is defined as

$$\Gamma=\frac{M_s}{A} \tag{2.6}$$

where M_s is the adsorbed mass of surfactant and A is the surface area. Surface tension decreases proportional to the surfactant concentration at the interface according to the equation of state derived from Langmuir adsorption [28].

$$\sigma=\sigma_s+RT\Gamma_\infty \ln\left(1\text{-}\frac{\Gamma}{\Gamma_\infty}\right), \tag{2.7}$$

where R is the ideal gas constant, T is the absolute temperature, σ_s is the surface tension of clean interface, and Γ_∞ is the maximum packing concentration. Equation (2.7) can also be written as

$$\sigma=\sigma_s\left[1+\beta_s\ln\left(1-\frac{\Gamma}{\Gamma_\infty}\right)\right], \tag{2.8}$$

where $\beta_s=RT\Gamma_s/\sigma_s$ is the elasticity number. The physicochemical parameter β_s is a measure of the sensitivity of interfacial tension to variations in surfactant concentration. Equation (2.8) is slightly modified to avoid negative values of the surface tension at high interfacial concentrations as

$$\sigma=\sigma_s\left\{\max\left[\varepsilon_\sigma,1+\beta_s\ln\left(1-\frac{\Gamma}{\Gamma_\infty}\right)\right]\right\}, \tag{2.9}$$

where ε_σ is taken as 0.05 in the present study. Fig. (1) shows the change in surface tension with respect to interfacial surfactant coverage for various elasticity numbers.

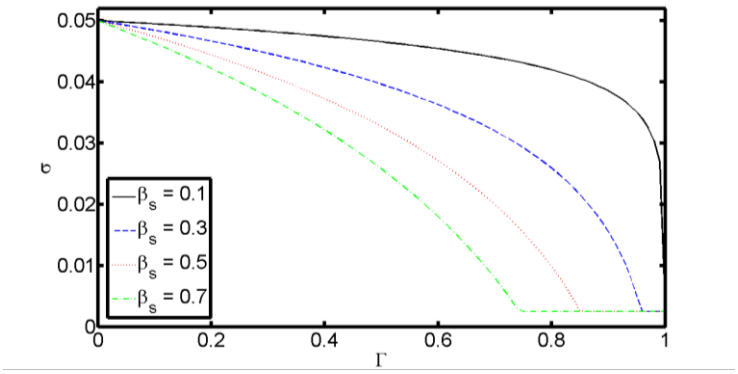

Figure 1: Surface tension for various elasticity numbers.

The surfactant concentration Γ evolves by,

$$\frac{\partial \Gamma}{\partial t} + \nabla_s \cdot (\Gamma \mathbf{U}_s) = D_s \nabla_s^2 \Gamma + \dot{S}_\Gamma, \tag{2.10}$$

where the gradient operator along the interface is defined as

$$\nabla_s = \nabla - \mathbf{n}(\mathbf{n} \cdot \nabla). \tag{2.11}$$

In Eq. (2.10) U_s is the tangential velocity on the interface, D_s is the diffusion coefficient along the interface and $\dot{S}_\Gamma$ is the source term given by

$$\dot{S}_\Gamma = k_a C_s(\Gamma_\infty - \Gamma) - k_b \Gamma, \tag{2.12}$$

where k_a and k_b are adsorption and desorption coefficients, respectively, and C_s is the surfactant concentration in fluid immediately adjacent to the interface. The bulk surfactant concentration C is governed by the advection-diffusion equation

$$\frac{\partial C}{\partial t} + \nabla \cdot (C\mathbf{u}) = \nabla \cdot (D_{co} \nabla C), \tag{2.13}$$

where the coefficient D_{co} is related to the molecular diffusion coefficient D_c and the indicator function I as

$$D_{co} = D_c[1 - I(r,z,t)], \tag{2.14}$$

The source term in eq. (2.10) is related to the bulk concentration as

$$\dot{S}_\Gamma = -D_{co}(\mathbf{n} \cdot \nabla C|_{\text{interface}}). \tag{2.15}$$

Following Muradoglu and Tryggvason [27], the boundary condition at the interface given by Eq. (2.15) is first converted into a source term in a conservative manner by assuming that all the mass transfer between the interface and the bulk takes place in a thin adsorption layer adjacent to the interface (See in Fig. 2). In this method, total amount of mass adsorbed on the interface is distributed over the adsorption layer and added to the bulk concentration evolution equation as a negative source term in a conservative manner.

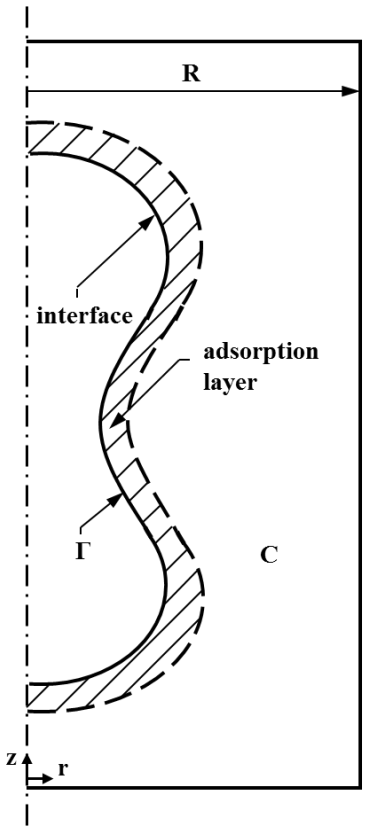

Figure 2: Schematic illustration of the adsorption layer

Equation (2.13) thus becomes

$$\frac{\partial C}{\partial t}+\nabla .(C\mathbf{u})=\nabla . (D_{co}\nabla C)+\dot{S}_C, \qquad (2.16)$$

where $\dot{S}_C$ is the source term evaluated at the interface and distributed onto the adsorption layer in a conservative manner. With this formulation, all the mass of the bulk surfactant to be adsorbed by the interface has been already consumed in the adsorption layer before the interface. Hence, the boundary condition at the interface simplifies to be $\mathbf{n}.\nabla C|_{interface}=0$.

2.2 Numerical Method

The flow equations are solved fully coupled with the evolution equations for interfacial concentration, Eq. (2.10), and for bulk concentration, Eq. (2.16), by the finite-difference/front-tracking method [27]. A first-order time integration method and a second-order centered difference approximation for the spatial derivatives are used to discretize the momentum and the continuity equations. The projection [30] method is used to solve the discretized equations on a stationary, staggered Eulerian grid. The bulk surfactant concentration and pressure are stored at the same location on the staggered grid. The evolution equation for the bulk surfactant concentration is solved fully coupled with the flow equations by using second-order centered differences for the spatial derivatives and a

first-order Euler method for the time integration. No-slip and no-flux boundary conditions are applied at the tube wall, while the symmetry is used at the tube centerline.

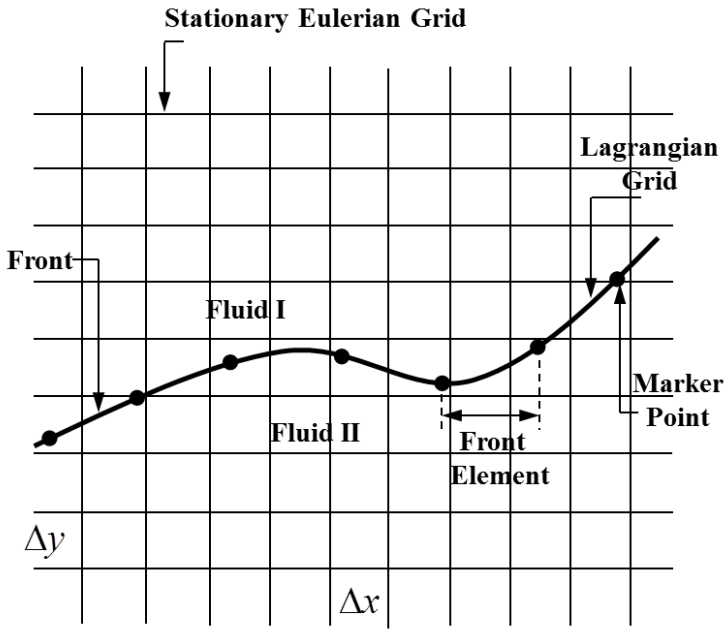

$$(h = \Delta x = \Delta y)$$

Figure 3: Schematic illustration of computational grids employed

To track the bubble-ambient fluid interface a separate Lagrangian grid is used. The Lagrangian grid consists of linked marker points (the front) that move with the local flow velocity interpolated from the stationary Cartesian Eulerian grid as sketched in Fig 3. The piece of the Lagrangian grid between two marker points is called a front element.

At each time step the indicator function defined by Eq. (2.5) is computed and is used to set the fluid properties inside and outside of the bubble. The indicator function is computed

on the Eulerian grid using the same procedure as described by Tryggvason et al. [32]. The method is briefly outlined here. The discontinuity is spread onto the grid points adjacent to the interface resulting in the gradient field

$$\mathbf{G}(x) = \nabla I = \int_A \mathbf{n}\delta(\mathbf{x}-\mathbf{x_f})dA, \tag{2.17}$$

which is zero everywhere except at the interface. Note that the vector field **G** is also utilized to enforce the no mass flux boundary condition for the bulk surfactant concentration at the interface as will be discussed in Sec. 2.2.3. Taking the divergence of both sides of Eq. (2.17) yields

$$\nabla^2 I = \nabla \cdot \mathbf{G}, \tag{2.18}$$

which is a separable Poisson equation and can be solved efficiently in the vicinity of the bubble. The delta function appearing in Eq. (2.17) is approximated by Peskin's cosine distribution function [31]. The same function is also used to distribute the surface tension forces at the center of front elements over the 16 neighboring grid points and also to interpolate the velocity vector from 16 Eulerian grid onto the marker points sketched in Fig. 4.

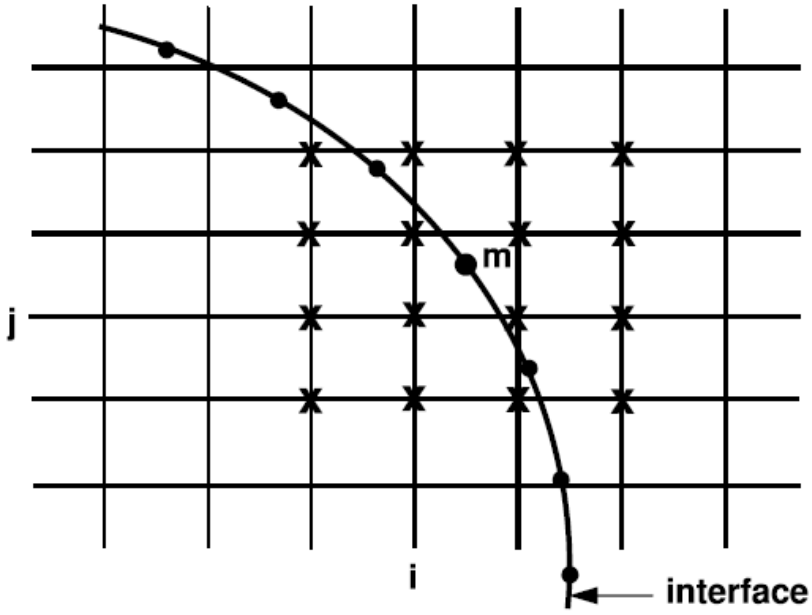

Figure 4: Sketch for interpolation scheme. Velocity is interpolated onto the location of m^{th} marker points from 16 neighboring Eulerian grid nodes. Similarly, the surface tension force computed at the front element centroid is distributed onto 16 neighboring Eulerian grid nodes.

In Eq. (2.18), the divergence operator is approximated using second-order central differences and then the Poisson equation is solved using a fast Poisson solver [33]. The computed indicator function is constant in each material region but with a finite-thickness transition zone at the interface. Therefore the transition region approximates a two-dimensional Heaviside function.

The interfacial surfactant concentration equation, Eq. (2.10), is solved on the Lagrangian grid by using second-order centered differences for the spatial derivatives and a first-order Euler method for the time integration. The Lagrangian grid is also used to find the surface tension, which is then distributed onto Eulerian grid points near the interface by

using Peskin's cosine distribution function [31], and added to the momentum equations as body forces as described by Tryggvason et al. [32].

The Lagrangian grid is restructured at every time step by deleting the front elements that are smaller than a prespecified lower limit and by splitting the front elements that are larger than a prespecified upper limit in the same way as described by Tryggvason et al. [32] to keep the front element size nearly uniform and comparable to the Eulerian grid size. Restructuring the Lagrangian grid is crucial since it avoids unresolved wiggles due to small elements and lack of resolution due to large elements. Note that restructuring the Lagrangian grid is performed such that the mass conservation is strictly satisfied for the surfactant at the interface. Since the finite-difference/front-tracking method has been described in details by Unverdi and Tryggvason [29] and by Tryggvason et al. [32] for surfactant-free flows, the basic flow solver is discussed only briefly here for completeness and emphasis is placed on the solution of the bulk and interfacial surfactant concentration evolution equations.

2.2.1 Flow Solver

The flow equations (Eqs. (2.1) and (2.2)) are solved on a stationary Eulerian grid. The spatial derivatives are approximated using second-order central finite-differences for all

field quantities. The time integration is achieved using a projection method. Following Unverdi and Tryggvason [29], Eqs. (2.1) and (2.2) are written in the form

$$\frac{\rho^{n+1}\mathbf{u}^{n+1}-\rho^{n}\mathbf{u}^{n}}{\Delta t}=\mathbf{A}^{n}-\nabla p, \tag{2.19}$$

$$\nabla\cdot\mathbf{u}^{n+1}=0, \tag{2.20}$$

where **A** is the advective, diffusive and body forces terms in Eq. (2.1). Then the above equation is decomposed as

$$\frac{\rho^{n+1}\mathbf{u}^{*}-\rho^{n}\mathbf{u}^{n}}{\Delta t}=\mathbf{A}^{n}, \tag{2.21}$$

$$\frac{\rho^{n+1}\mathbf{u}^{n+1}-\rho^{n+1}\mathbf{u}^{*}}{\Delta t}=-\nabla p, \tag{2.22}$$

where **u*** is a provisional velocity ignoring the effect of the pressure. Next the unprojected velocity field is computed from Eq. (2.21) and then the pressure field is computed as follows: taking the divergence of Eq. (2.22) and using the incompressibility condition given by Eq. (2.20), we obtain a non-separable Poisson equation for pressure in the form

$$\nabla\cdot\frac{1}{\rho^{n+1}}\nabla p=-\frac{1}{\Delta t}\nabla\cdot\mathbf{u}^{*}, \tag{2.23}$$

which is solved on the Eulerian grid using a multigrid method as described by Tryggvason et al. [32]. Finally the velocity field at the new time level is computed as

$$\mathbf{u}^{n+1}=\mathbf{u}^{*}-\frac{\Delta t}{\rho^{n+1}}\nabla p, \tag{2.24}$$

2.2.2 Surfactant Concentration at the Interface

The evolution equation of the surfactant concentration at the interface is solved on the Lagrangian grid. From Eqs. (2.10) and (2.11) we obtain

$$\frac{\partial \Gamma}{\partial t}+\nabla\cdot(\Gamma \mathbf{U}_s)-\Gamma \mathbf{n}\cdot\nabla \mathbf{U}_s\cdot\mathbf{n}= D_s\nabla_s^2\Gamma+\dot{S}_\Gamma. \tag{2.25}$$

On the other hand, the area of an element of the interface evolves by [34]

$$\frac{DA}{Dt}= \frac{\partial A}{\partial t}+ \mathbf{U}_s\cdot\nabla A= -A(\mathbf{n}\cdot\nabla \mathbf{u}\cdot\mathbf{n}). \tag{2.26}$$

Combining Eqs. (2.25) and (2.26), one obtains

$$\frac{d\Gamma A}{dt}=AD_s\nabla_s^2\Gamma+A\dot{S}_\Gamma. \tag{2.27}$$

For an axisymmetric problem, Eq. (2.27) can be written as

$$\frac{d\Gamma A}{dt}=A\left(D_s\frac{1}{r}\frac{\partial}{\partial s}\left(r\frac{\partial \Gamma}{\partial s}\right)+\dot{S}_\Gamma\right), \tag{2.28}$$

where s is the arc length along the interface and r is the radial coordinate in cylindrical coordinates. Equation (2.28) can be expressed in compact form as

$$\frac{d\Gamma A}{dt}=Af(\Gamma,t), \tag{2.29}$$

where f is given by

$$f(\Gamma,t)= D_s\frac{1}{r}\frac{\partial}{\partial s}\left(r\frac{\partial \Gamma}{\partial s}\right)+\dot{S}_\Gamma. \tag{2.30}$$

2.2.3 Bulk Surfactant Concentration

The bulk surfactant concentration equation is solved on the staggered Eulerian grid. The bulk surfactant concentration is located at the pressure nodes. The spatial derivatives are approximated using second-order central differences and time integration is performed using a first-order explicit Euler method. The source term is first computed on the interface and is then distributed over the adsorption layer in conservative manner. For this purpose, the distribution algorithm is slightly modified as follows: the source term $\dot{S}_{C_{i,j}}$ at grid point (i,j) is approximated as

$$\dot{S}_{C_{i,j}} = -\sum_{k} \omega_{i,j}^{k} \dot{S}_{\Gamma_k} \frac{r_k \Delta l_k}{r_{i,j} h^2}, \tag{2.31}$$

where $\dot{S}_{\Gamma_k}$ is the source term evaluated at the center of the k^{th} element, r_k and Δl_k are the radial coordinate of the center and the arc length of the k^{th} element, $r_{i,j}$ is the radial coordinate of the grid node (i,j), h is the grid spacing and $\omega_{i,j}^{k}$ is the weight of grid point (i,j), respectively. The weight must satisfy the consistency condition

$$\sum_{i}\sum_{j} \omega_{i,j}^{k} = 1, \tag{2.32}$$

in order to conserve the total source strength in going from the interface to the grid. The weight for the grid point (i,j), for smoothing from the center of the k^{th} element (r_f^k, z_f^k), can be written as

$$\omega_{i,j}^{k} = \frac{\widetilde{\omega}_{i,j}^{k}}{\sum_i \sum_j \widetilde{\omega}_{i,j}^{k}}, \tag{2.33}$$

where the non-normalized weight function is defined as

$$\widetilde{\omega}_{i,j}^{k} = d_c\left(r_f^k - ih\right) d_c\left(z_f^k - jh\right). \tag{2.34}$$

In Eq. (2.34), the distribution function d_c is a slightly modified version of the Peskin's cosine distribution defined as

$$d_c(x) = \begin{cases} \frac{1}{W}\left(1 + \cos\left(\frac{\pi x}{W}\right)\right) & \text{if } |x| < W \text{ and } I < 0.5 \\ 0, & \text{otherwise,} \end{cases} \tag{2.35}$$

where W is the width of the adsorption" layer, taken as $W = 2h$ in the present study ($h = \Delta x$ is the grid size). As can be seen in Eq. (2.35), the source term is distributed only outside of the bubble region, i.e., $I(r,z,t) \leq 0.5$, which is illustrated schematically in Fig. 5.

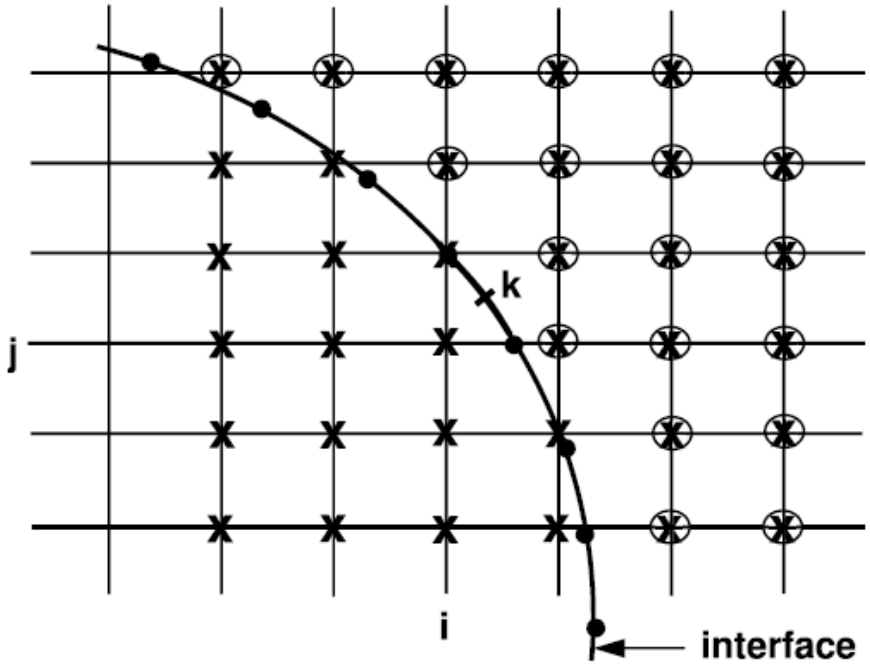

Figure 5: Sketch for interpolation scheme. The bulk surfactant concentration is interpolated from the Eulerian grid nodes outside of the bubble onto k^{th} front element and the source term computed on the front element is distributed onto the same Eulerian grid nodes.

2.3 Problem Statement

The physical problem and computational domain are sketched in Fig. 6. The computational domain is R in radial direction and L_z in the axial direction. The lower boundary is the axis of symmetry which represents the centerline of the channel and the flow is in the axial direction. The bubble is initially located at the channel centerline close to the inlet section. The bubble is much longer than the channel width and are initialized with an approximate shape of a straight middle portion and semi-circular front and back menisci. The thickness of the film between the bubble and the wall is initialized according to the Taylor's Law [1]

$$\frac{h_\infty}{R} = \frac{1.34Ca^{2/3}}{1+1.34 \text{ x } 2.5Ca^{2/3}}. \qquad (2.36)$$

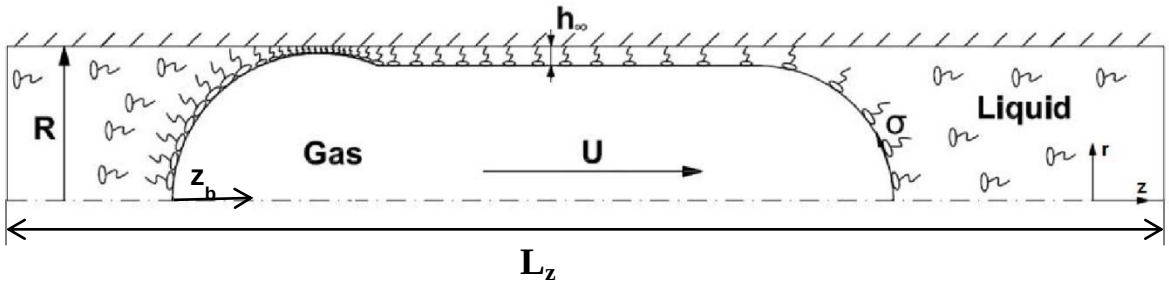

Figure 6: Schematic illustration of the computational setup for a bubble moving in a horizontal axisymmetric channel with soluble surfactant.

The flow is initiated instantaneously by imposing a fully-developed steady flow at the inlet and keeping the pressure constant at the outlet. Symmetry and no-slip boundary conditions are used at the centerline and at the wall of the tube, respectively. The computational domain is set sufficiently long e.g., (L_z /R=100) to ensure steady state motion of bubbles. To study the effects of surfactant on the liquid film thickness between the wall and the bubble moving in an axisymmetrical channel, computations are performed for three different cases: soluble, insoluble and clean. In all the three cases, the same effective surface tension coefficient, σ_{eff}, is utilized, which is first calculated in the soluble case as

$$\sigma_{eff}=\sigma_s\left\{\max\left[\varepsilon_\sigma, 1+\beta_s \ln\left(1-\frac{\Gamma_{ave}}{\Gamma_\infty}\right)\right]\right\} \tag{2.37}$$

where Γ_{ave} is the average surfactant concentration obtained at the end of the simulation in the soluble case.

In the soluble surfactant case, the initial bulk surfactant concentration is specified uniformly as C_∞ which is initial bulk surfactant concentration value and the initial interfacial surfactant concentration, Γ_0, is specified to be 80% of the interfacial equilibrium surfactant concentration, Γ_{eq} . In equilibrium, the adsorption equals to the desorption; hence we calculate Γ_{eq} by equating the source term in Eq. (2.12). In the insoluble surfactant case, the bulk fluid is surfactant free and the initial interfacial surfactant concentration, Γ_0, is specified to be approximately the steady-state average interfacial surfactant concentration in the soluble case, i.e., $\Gamma_0 = \Gamma_{ave}$. Finally, in the clean case, both the bulk fluid and the

interface are surfactant free. In both the insoluble and clean cases, σ_{eff} is utilized in the computations, which is calculated according to Eq. (2.37). In all cases the relevant non-dimensional numbers are kept the same.

The governing equations given in Sec 2.1 are solved in their dimensional forms, and the results are expressed in terms of relevant non-dimensional quantities. The governing non-dimensional numbers can be summarized as

$$\mathrm{Re}=\frac{\rho_o U R_c}{\mu_o},\quad \mathrm{Pe_c}=\frac{U R_c}{D_c},\quad \mathrm{Pe_s}=\frac{U R_c}{D_s},\quad \frac{\rho_b}{\rho_o},\quad \frac{\mu_b}{\mu_o},$$

$$\mathrm{k}=\frac{k_a C_\infty}{k_b},\ \mathrm{Bi}=\frac{k_b R_c}{U},\ \mathrm{Da}=\frac{\Gamma_\infty}{R_c C_\infty},\ \beta_s=\frac{RT\Gamma_\infty}{\sigma_s},\ \mathrm{Ca_{eff}}=\frac{\mu U_b}{\sigma_{eff}}, \tag{2.38}$$

where Re, $\mathrm{Pe_c}$, $\mathrm{Pe_s}$, k, Bi, Da, are the Reynolds number, the Peclet number based on bulk surfactant diffusivity, the Peclet number based on interface surfactant diffusivity, the dimensionless adsorption depth, the Biot number, the Damkohler number, and the elasticity number, respectively.

We defined a base case and chose the non-dimensional parameters of this base case to approximately represent the physical conditions of a neonatal's lower airways. The non-dimensional numbers are taken as; Re = 1, $\mathrm{Pe_c}$ = 100, $\mathrm{Pe_s}$ = 1000, ρ_b/ρ_o = 1, μ_b/μ_o = 0.1, k = 1, Bi = 0.02, Da = 0.1, β_s = 0.5 and $\mathrm{Ca_{eff}}$ = 0.0125. The Re and Ca number is generally low, e.g., (Re ≅ 0.1) in the lower airways [35] and we have chosen a representative value of Re = 1 and Ca = 0.0125. Note that Aussillous and Quere [1] showed that Reynolds

number effects are negligible when Re<10. Pe_c and Pe_s are taken as Pe_c = 100 and Pe_s = 1000 following Fujioka and Grotberg [35]. Adsorption and desorption coefficients for pulmonary surfactant are given as $k_a = 1.7 \times 10^{-3}$ cm^3 g^{-1} s^{-1} and $k_b = 1.7 \times 10^{-2}$ s^{-1} [36, 37]. Generally the maximum equilibrium interfacial surfactant concentration for the pulmonary surfactant is about 10^{-3} times maximum bulk surfactant concentration which is practically the critical micelle bulk concentration for the pulmonary surfactant [38, 39]. Therefore we assume that C_∞ = 10 g cm^{-3} and $\Gamma_\infty = 3.1 \times 10^{-2}$ g cm^{-2}. The non-dimensional adsorption depth is calculated accordingly as k = 1. Elasticity number is taken as 0.5 following Ghadiali and Gaver [11]. The radius of the lower generations of the lung is 0.014 cm [40]. Therefore the Damkohler number is accordingly calculated to be Da = 0.071 and we take Da = 0.1.

We employed a uniform regular Cartesian grid and performed grid convergence study to ensure that the results are independent of spatial grid. These studies, as detailed in the Appendix, indicated that 32 grid cells in the radial direction are sufficient to keep the error in film thickness and interfacial surfactant concentration below 4% and 7%, respectively.

Chapter 3

RESULTS AND DISCUSSION AND CONCLUSION

3.1 Validation

To validate the numerical method, the film thickness computed for the clean case interface is first compared with Taylor's Law which is a semi-analytic expression [21] given by Eq. (2.36). As shown in Fig. 7 our numerical results fit well to the Taylor's Law, indicating the accuracy of the numerical method. Computations are performed on grids for which the film region is resolved at least by 4 grid points, which is sufficient to reduce the numerical error below 5%.

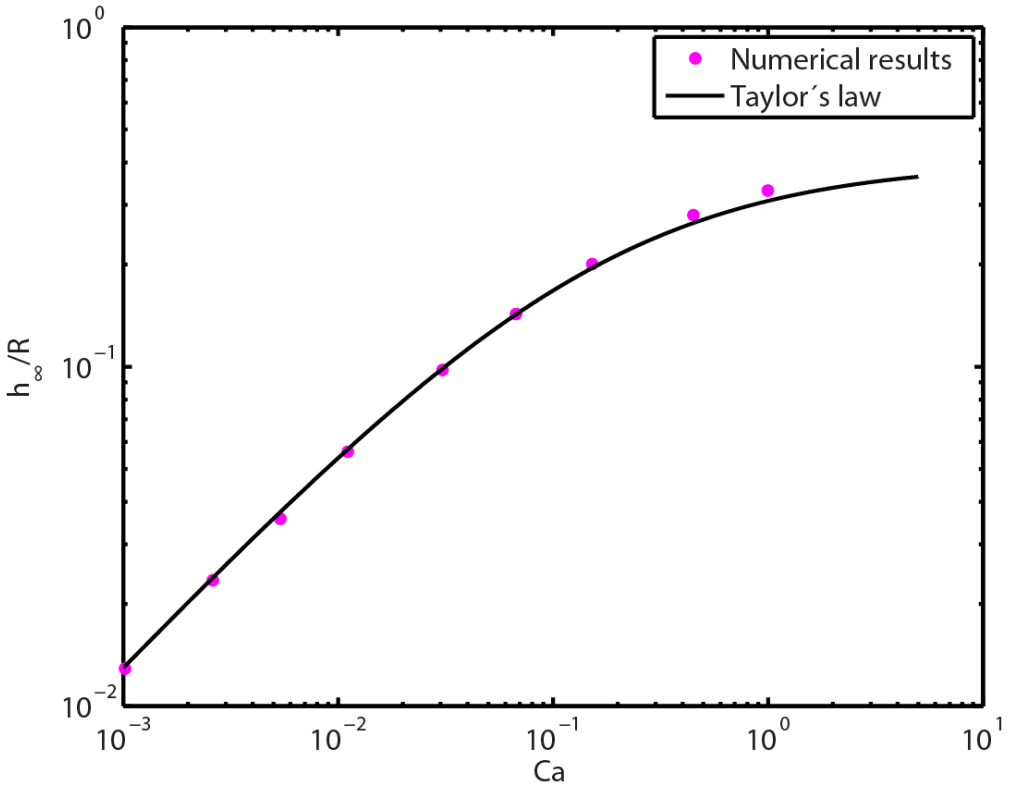

Figure 7: Film thickness for the clean bubble. Solid line is Taylor's Law and symbols are the present results.

3.2 Effects of Surfactant

After the validation study of the method for the clean case, we added surfactant to our system and performed computations. The film thickness and interfacial surfactant distribution for the clean, insoluble and soluble base cases, i.e., Ca_{eff}=0.0125, are compared in Fig. 8.

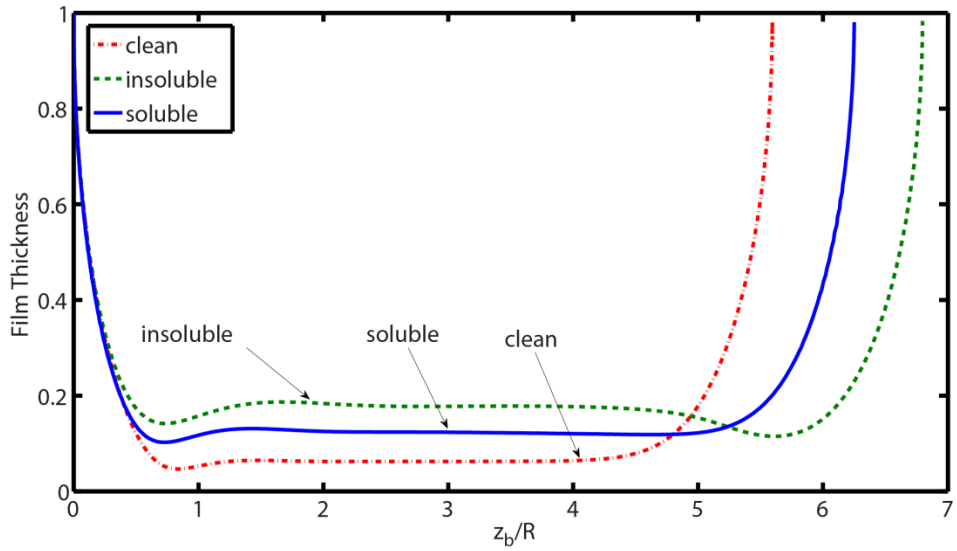

(a)

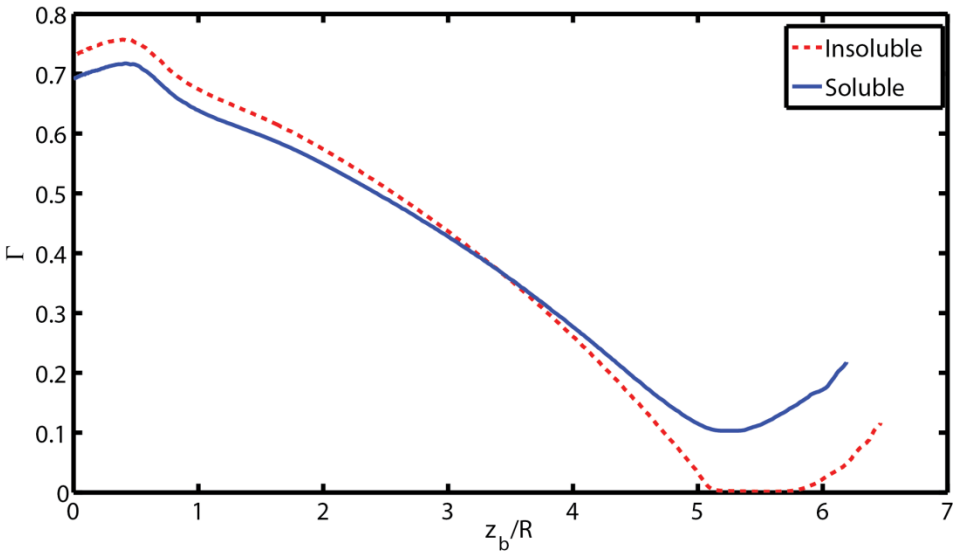

(b)

Figure 8: Comparison of three cases. (a) The film thickness and (b) The interfacial surfactant distribution. (Caeff=0.0125)

It is observed in Fig. 8a that the surfactant generally thickens the liquid film and the film thickness of the insoluble surfactant case is larger than the film thickness of the soluble surfactant case. The reason of this is the distribution of the surfactant on the interface, which is shown in Fig. 8b. In both the soluble and the insoluble cases, surfactants at the leading edge of the bubble are convected to the liquid film and the trailing edge of the bubble. However, in the insoluble case, there is no surfactant transfer from bulk to the interface. Therefore, the surfactant concentration at the leading edge of the bubble in the insoluble case is nearly zero as seen in Fig. 8b. Surface tension at the leading edge in the insoluble case does not decrease due to the absence of surfactant, and hence we observe an expanded leading edge in the insoluble case compared to the soluble one, as shown in Fig. 8a. This expansion in the leading edge stretches the bubble in the axial direction and results in an increase in the liquid film thickness.

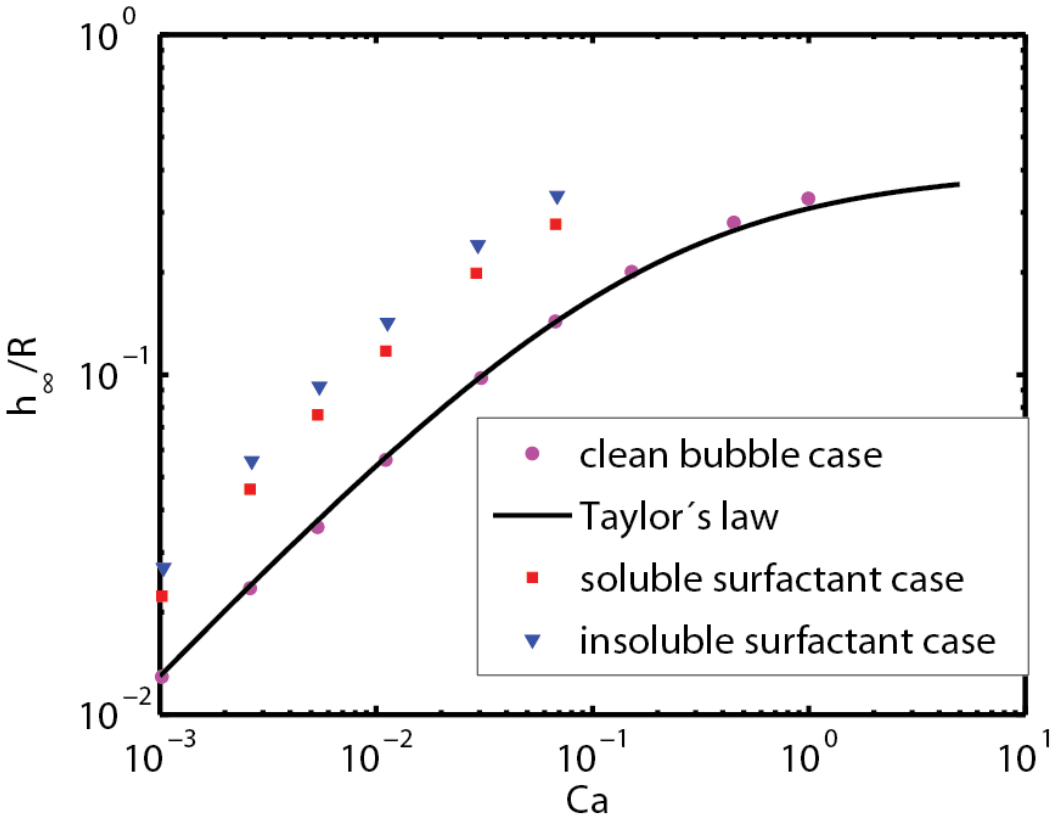

Figure 9: Film thicknesses for the clean, insoluble and soluble cases. Solid line is Taylor's Law and circles, squares and triangles represent clean, soluble and insoluble cases, respectively.

We next examine the effects of surfactant on the steady film thickness both for the insoluble and soluble cases. Fig. 9 shows the variation of film thickness as a function of Capillary number. As can be seen in this figure, surfactant generally increases the film thickness. It is interesting to observe that insoluble surfactant model yields consistently higher film thickness than the soluble model for all Capillary numbers.

It is observed that when surfactant is added to the system, the velocity of the bubble increases. The reason for this behavior is that as the surfactant thickens the liquid film, the bubble shifts more into the faster flowing inner core of the fluid. As expected, velocity of the bubble in the insoluble surfactant case is the highest of all the three cases, whereas, in the clean case, it is the slowest. Velocities of three cases are; $(U_b/U)_{clean}$ = 1.11, $(U_b/U)_{insoluble}$ = 1.15, $(U_b/U)_{soluble}$ = 1.13

Surfactant concentration distribution in the bulk fluid and the interfacial surfactant distribution are shown in Fig. 10 at various times to demonstrate the unsteady evolution of these distributions. It is observed that the bulk surfactant close to the centerline on the leading edge is consumed.

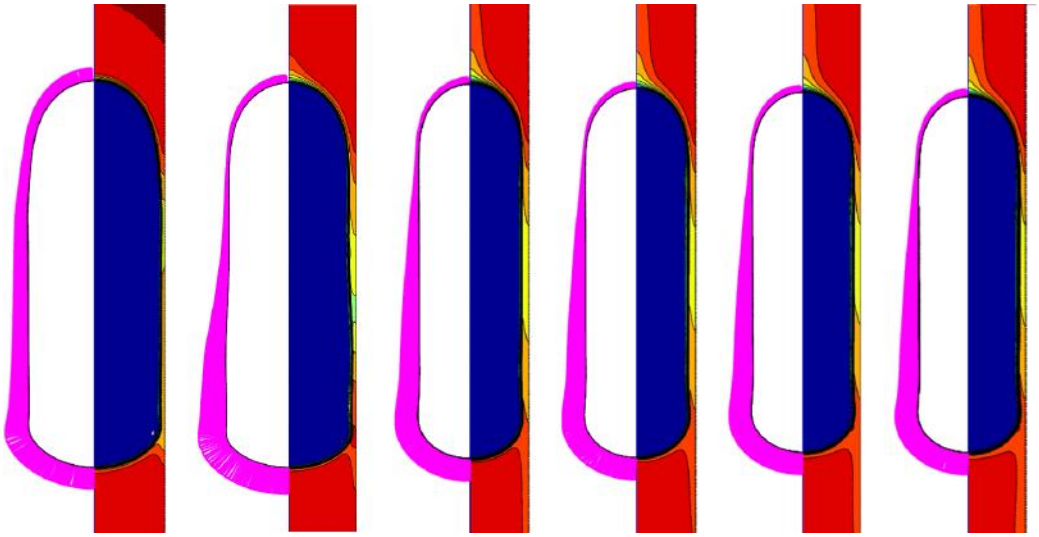

Figure 10: Evolution of surfactant concentration at the interface (left side) and in the bulk fluid (right side). From left to right z/L = 0.0481, 0.0962, 0.2500, 0.4423, 0.7154, 0.9231.

The streamlines in Fig. 11 explain this phenomenon: The circulation on the leading edge of the bubble brings the surfactant in the vicinity of the wall to the leading edge of the bubble. As it sweeps the leading edge, the surfactant is being consumed and the bulk concentration in the vicinity of the centerline decreases. The interfacial surfactant concentration assumes its minimum value at the stagnation point on the leading edge and increases until the other stagnation point at the trailing edge, where it makes a maximum (Fig. 8b) (The stagnation points are shown in Fig. 11). Along these two stagnation points, the bulk concentration is decreased as shown in Fig. 10. The second circulation at the trailing edge brings the bulk surfactant along the centerline to the trailing edge of the bubble and is the reason for the maximum interfacial surfactant concentration at the stagnation point on the trailing edge.

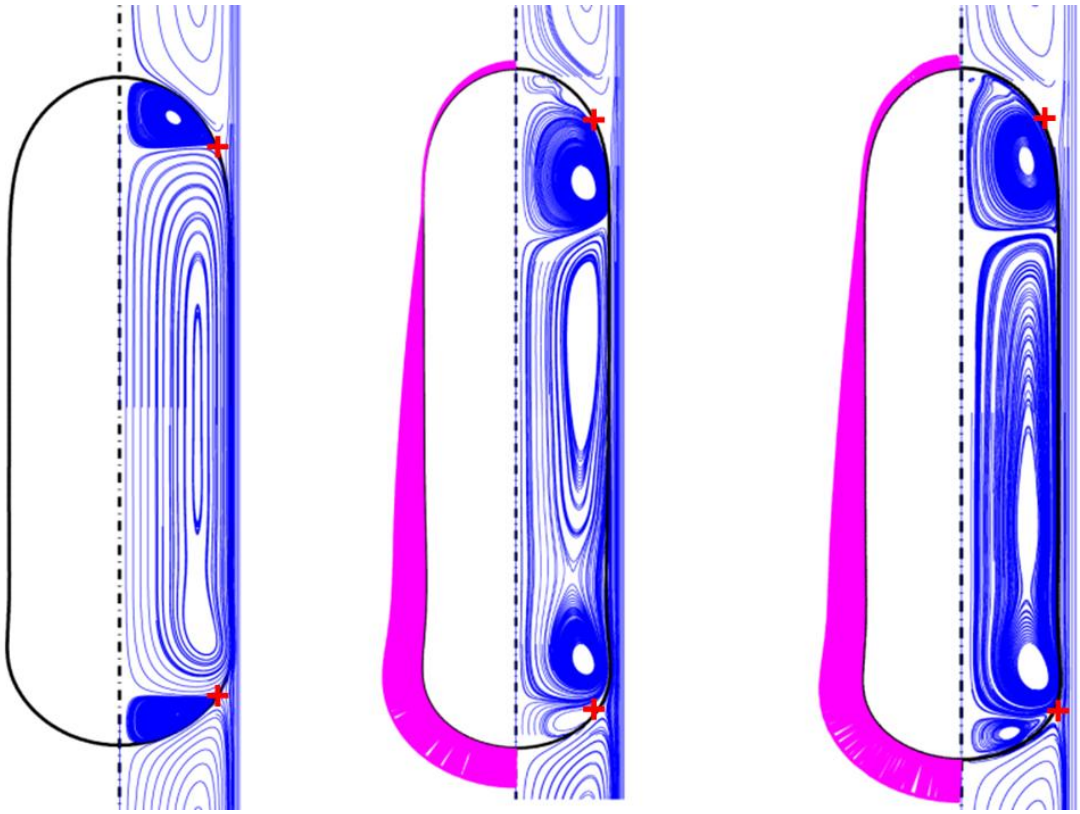

Figure 11: Streamlines for the three cases and interfacial surfactant distribution for the insoluble surfactant and the soluble surfactant cases. Left is the clean case, middle is the insoluble surfactant case and the right is the soluble surfactant case. Red pluses represent stagnation points.

3.3 Effects of Non-dimensional Parameters

3.3.1 Effects of Elasticity Number

Computations are performed to examine the effect of elasticity number on the motion of a large bubble in a capillary tube for the soluble surfactant case. For this purpose, the elasticity number, β_s is varied between 0.1 and 0.7 while other parameters are kept the same as the base case. In Fig. 12, the bubble interface is shown together with the contour plots of the constant surfactant concentration in the bulk fluid and the surfactant concentration distribution along the interface for β_s = 0.1, 0.3, 0.5 and 0.7 at steady state.

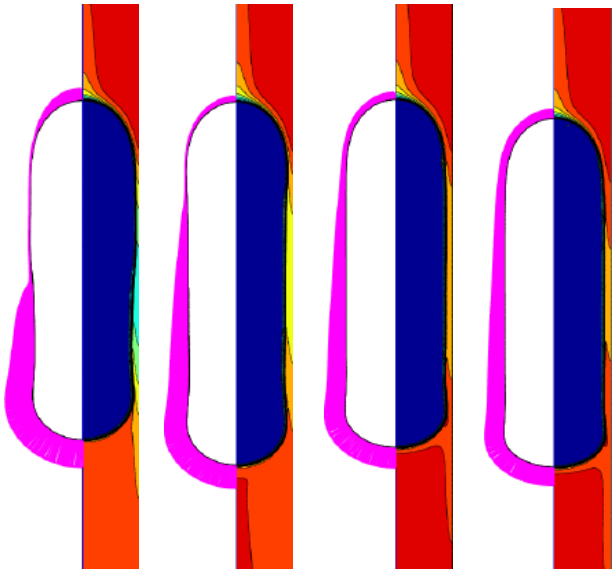

Figure 12: Effects of Elasticity number on the bulk surfactant distribution. Bulk and interface surfactant distributions are plotted for various β_s values. (From left to right β_s = 0.1, β_s = 0.3, β_s = 0.5, β_s = 0.7).

When β_s increases, surface tension decreases more abruptly with increasing interfacial surfactant concentration (see Fig. 1), and this results in an increase in Marangoni stresses, which causes the mobility of the interface to decrease. Because of this, the interfacial surfactant on the leading meniscus cannot be advected to the trailing meniscus and interfacial concentration becomes relatively uniform. Conversely, as β_s decreases, surface tension is less sensitive to interfacial surfactant concentration and this result in lower Marangoni stresses and higher mobility of the interface. Therefore, interfacial surfactant on the leading meniscus are easily advected along the interface and accumulated at the trailing meniscus of the bubble. Due to this accumulated mass at $\beta_s = 0.1$, surface tension becomes very small at the back of the bubble and this causes the film thickness at this location to be thicker. However, at the front of the bubble, surfactant concentration is close to zero; hence the front of the bubble behaves like a clean bubble as shown in Fig. 13a. As β_s increases, surfactant distribution at the interface becomes more uniform which can be seen in Fig. 13b. Therefore, surface tension values of the interface become more uniform. This makes the film thickness to be same at the front and back of the bubble that is shown in Fig. 13a.

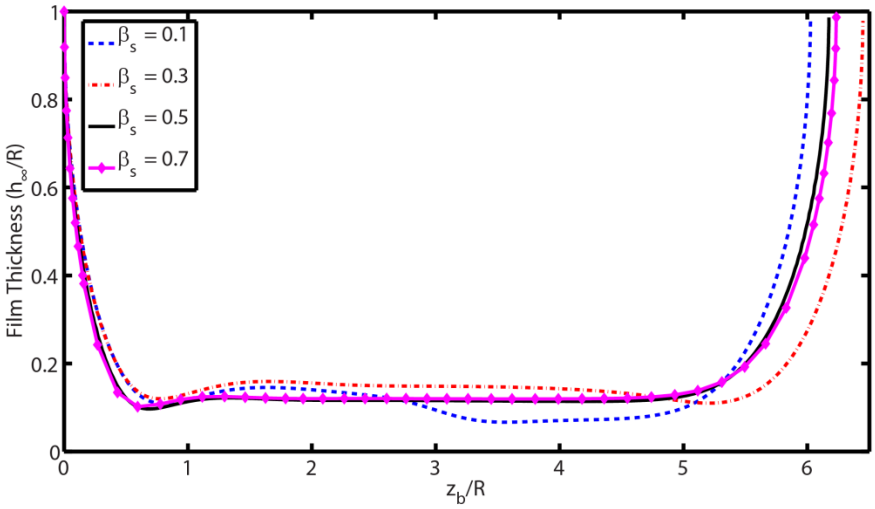

(a)

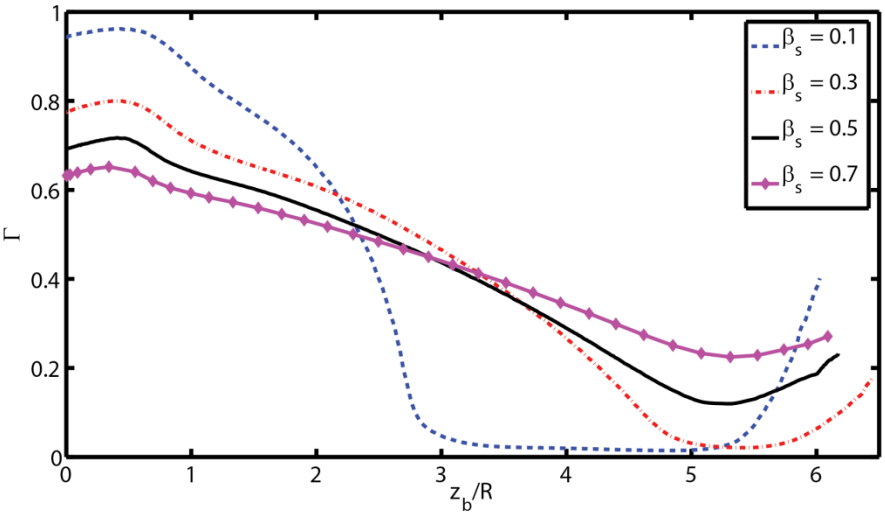

(b)

Figure 13: Effects of Elasticity number on the (a) film thickness and (b) interfacial surfactant concentration. Film thickness of bubble and interfacial surfactant concentrations are plotted for various β_s values.

3.3.2 Effects of Peclet Number

In order to investigate the effects of surface Peclet (Pe_s) and bulk Peclet (Pe_c) numbers computations are carried out for Pe_s and Pe_c values in the range (10 - 10^4) and (3 - 10^3), respectively, while other parameters are kept the same as the base case. Surface and bulk Peclet numbers are varied together proportionally. In Fig. 14, bulk and interfacial surfactant concentrations are displayed for various Peclet numbers. As Pe numbers increase (decrease) the thickness of the mass transfer boundary layer decreases (increases), which was also observed by Ghadiali and Gaver [11]. As Pe numbers increase, convection becomes dominant over diffusion, which causes the bulk surfactant concentration to have a sharp gradient in the vicinity of the interface. However, the steady state interfacial surfactant distribution is only slightly responsive to the changes in Pe numbers as shown in Fig. 15b. The change in interfacial surfactant concentration with Pe numbers shows a non-monotonic behavior, which in turn causes the film thickness to show a non-monotonic behavior. We have observed the maximum film thickness for about Pe_s = 100 as shown in Fig. 15a, which is qualitatively in agreement with the results of Ghadiali and Gaver [11].

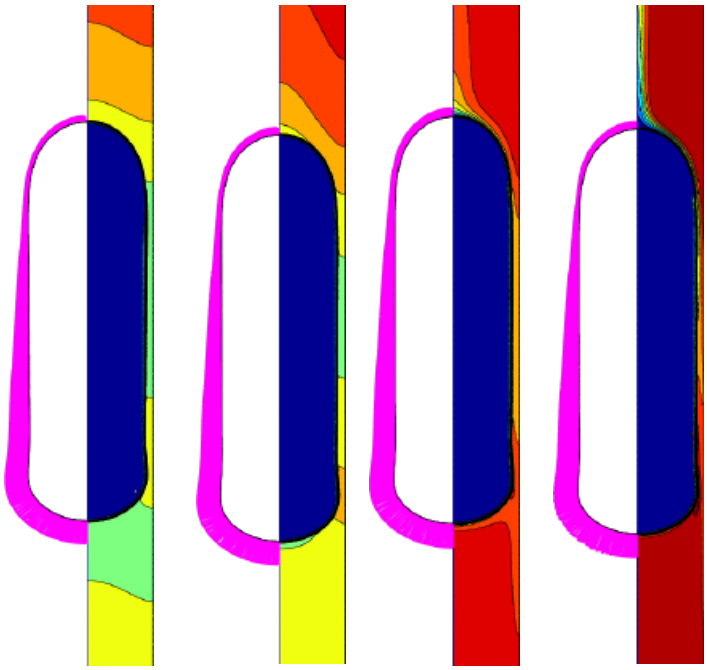

Figure 14: Effects of Peclet number on the bulk surfactant distribution. Bulk and interface surfactant distributions are plotted for various Peclet values. (From left to right (Pe_s = 10, Pe_c = 3), ($Pe_s = 10^2$, Pe_c = 10), ($Pe_s = 10^3$, $Pe_c = 10^2$), ($Pe_s = 10^4$, $Pe_c = 10^3$)).

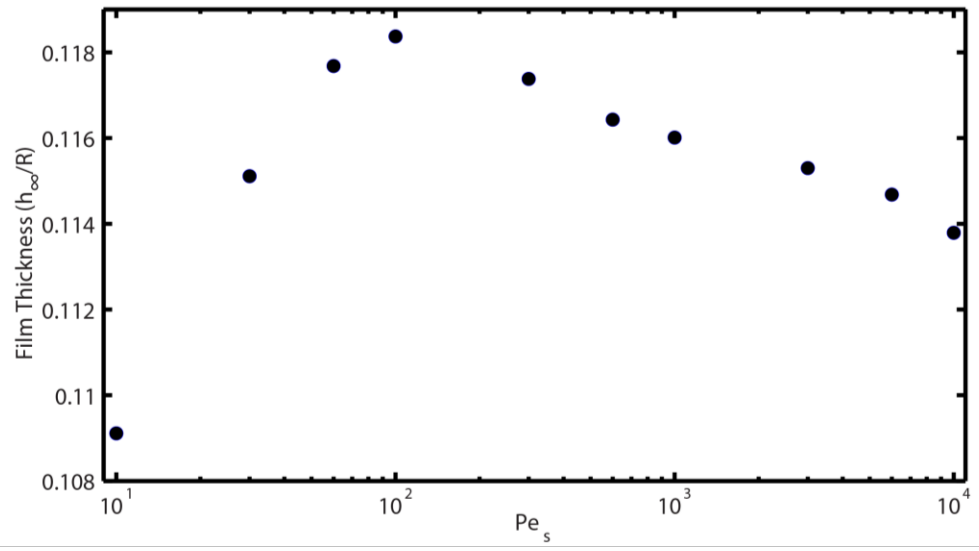

(a)

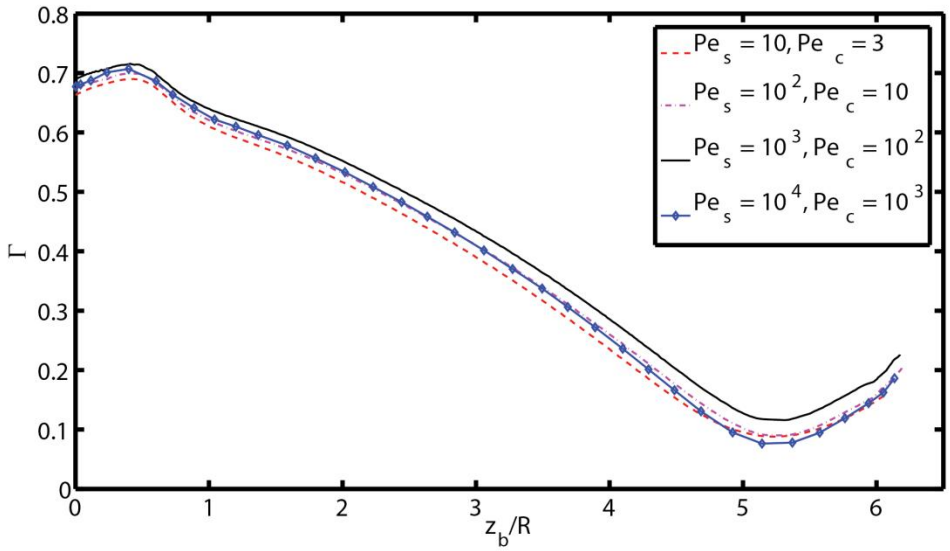

(b)

Figure 15: Effects of Peclet number on the (a) film thickness and (b) interfacial surfactant concentration. Film thickness of bubble and interfacial surfactant concentrations are plotted for various Peclet values.

3.3.3 Effects of Damkohler Number

In order to investigate the effects of Damkohler number, computations are performed for Da numbers in the range of 0.033 – 1. We also varied the dimensionless adsorption depth, k, proportionately, in order to keep the adsorption-desorption coefficients ratio constant. In this manner, we practically change only the initial bulk surfactant concentration C_∞. All the other non-dimensionless parameters are kept the same as the base case. In Fig. 16, bulk and interfacial surfactant concentrations are displayed. As Da number increases (decreases), the thickness of the mass transfer boundary layer increases (decreases). This is because at low Da numbers, the initial bulk surfactant concentration is high, which causes the bulk surfactant only in the very vicinity of the interface suffice to fill up the interface. Conversely, at high Da numbers, the initial bulk surfactant concentration is low and bulk surfactant not only in the vicinity of the interface, but also distant from the interface are absorbed on it. At low Da numbers, i.e., Da = 0.033, the interfacial surfactant concentration is more uniform compared to the base case (Da = 0.1), which is because of the higher bulk surfactant concentration. The higher interfacial concentration leads to lower surface tension on the interface and correspondingly increased film thickness as shown in Fig. 17. On the other hand at higher Da numbers, e.g., Da = 0.2, the interfacial surfactant concentration on the leading meniscus is negligible and the

resulting increased surface tension makes the leading meniscus to bulge into a spherical shape. This leads to an increased film thickness –maximum among various Da number cases- in the middle portion of the bubble. Further increase in Da number pulls the close-to-zero interfacial concentration region back and close to the trailing edge. This increases the size of the region that tends to grow into a spherical shape (not only the leading meniscus, but all the bubble except for the trailing meniscus). This tendency decreases the film thickness in the middle portion of the bubble (See Da = 1 case in Fig. 17a.)

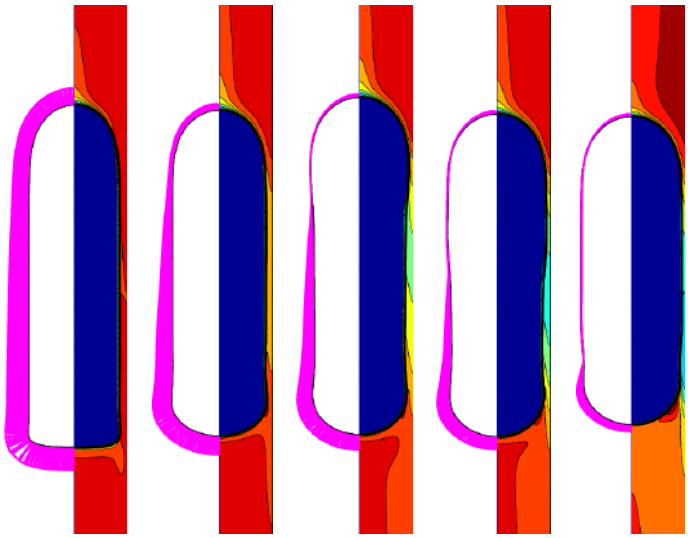

Figure 16: Effects of Damkohler number on the bulk surfactant distribution. Bulk and interface surfactant distributions are plotted for different Damkohler values. Besides Damkohler number, k(dimensionless adsorption depth) is changed to keep adsorption-desorption ratio constant. (From left to right (Da = 0.033, k = 3), (Da = 0.1, k = 1), (Da = 0.2, k = 0.5), (Da = 0.33, k = 0.3), (Da = 1, k = 0.1)).

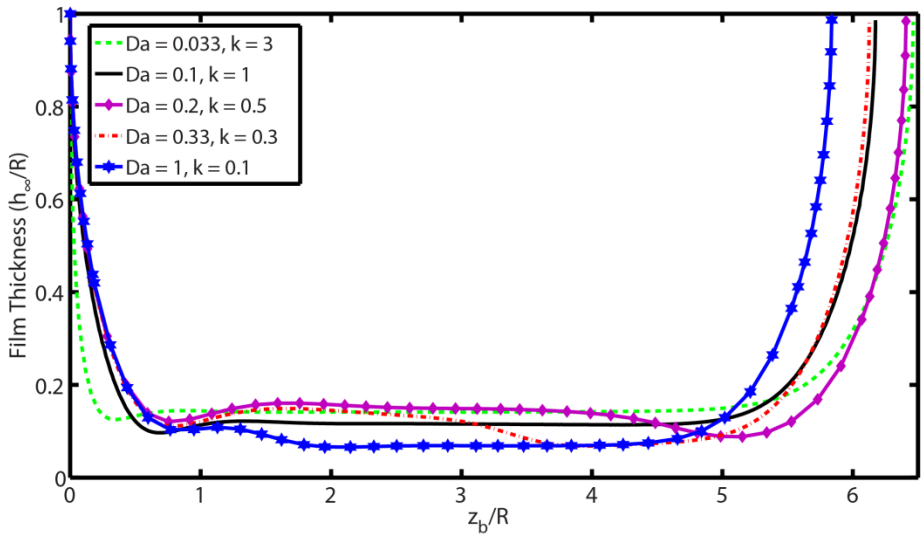

(a)

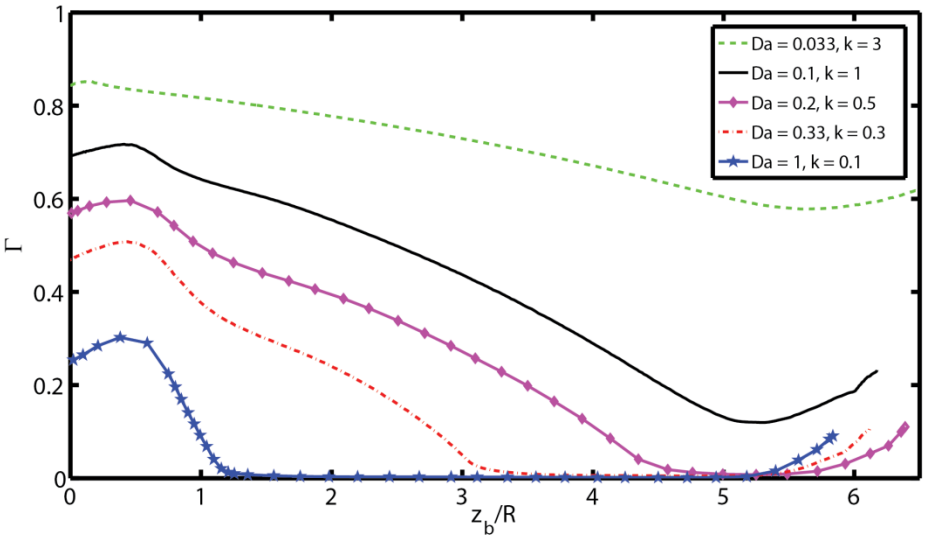

(b)

Figure 17: Effects of Damkohler number on the (a) film thickness and (b) interfacial surfactant concentration. Film thickness and interfacial surfactant concentration are plotted for various Damkohler values. Besides Damkohler number, k (dimensionless adsorption depth) is changed to keep adsorption-desorption ratio constant.

Chapter 4

CONCLUSION

The effects of soluble and insoluble surfactants on the motion and deformation of a gas bubble in a horizontal axisymmetric channel are computationally studied by using a finite-difference/front-tracking method. The Navier–Stokes equations are solved fully coupled with the bulk and interfacial surfactant concentration evolution equations, and the surface tension is related to the interfacial surfactant concentration using a nonlinear equation of state based on the Langmuir kinetics. Computations are performed to study the effects of insoluble and soluble surfactants on liquid film thickness and terminal velocity of the bubble. It is found that the presence of surfactants increases the liquid film thickness, which compares qualitatively well with the experimental findings of Krechetnikov and Homsy [2]. It is also shown that when soluble or insoluble surfactants are added to the fluid, the terminal velocity of the bubble increases.

Further computations are performed to examine the effects of the non-dimensional numbers in insoluble and soluble surfactant cases. It is found that β_s and Da have a

profound influence on the bubble dynamics. Both parameters significantly change the surfactant concentration distribution on the interface. As β_s increases, the surface mobility significantly decreases due to increasing Marangoni stresses and correspondingly, liquid film thickness becomes more uniform. Conversely, as β_s decreases, surfactants accumulate only at the trailing meniscus, which results in a non-uniform film thickness. Also, Da has significant influence on the surfactant distribution at the surface. While Da increases (decreases), bulk surfactant concentration and the interfacial surfactant concentration decreases (increases). This change in the surface surfactant distribution directly affects the film thickness. Pe numbers effect on the film thickness is relatively weaker and is non-monotonic.

APPENDIX

Three sets of uniform regular Cartesian grids with 32, 64 and 128 grid cells in the radial direction are used to solve the governing equations for flow and surfactant transport. Comparisons are made on the converged steady-state results of interfacial surfactant distribution and film thickness. Fig. (24) shows the discrepancy in interfacial surfactant distribution along bubble arc length for these three different grid systems. The relative error is defined as follows:

$$\varepsilon = \frac{|\text{Numerical value} - \text{Exact value}|}{\text{Exact value}} \tag{A1}$$

For every grid system, three different values from three different locations are collected. These values are plotted and a first-order spline is fitted to these values. The value as grid size goes to zero is assumed to be the exact value.

The grid with 32 grid cells in radial direction was sufficient to resolve all flow features and to accurately calculate interfacial surfactant distribution within a relative error margin of 7% compared with the grid with 64 grid cells. Three different locations in Fig. 18 is chosen to test the accuracy of the numerical schemes employed. As can be seen in Fig. 18, surface surfactant distribution is second order accurate.

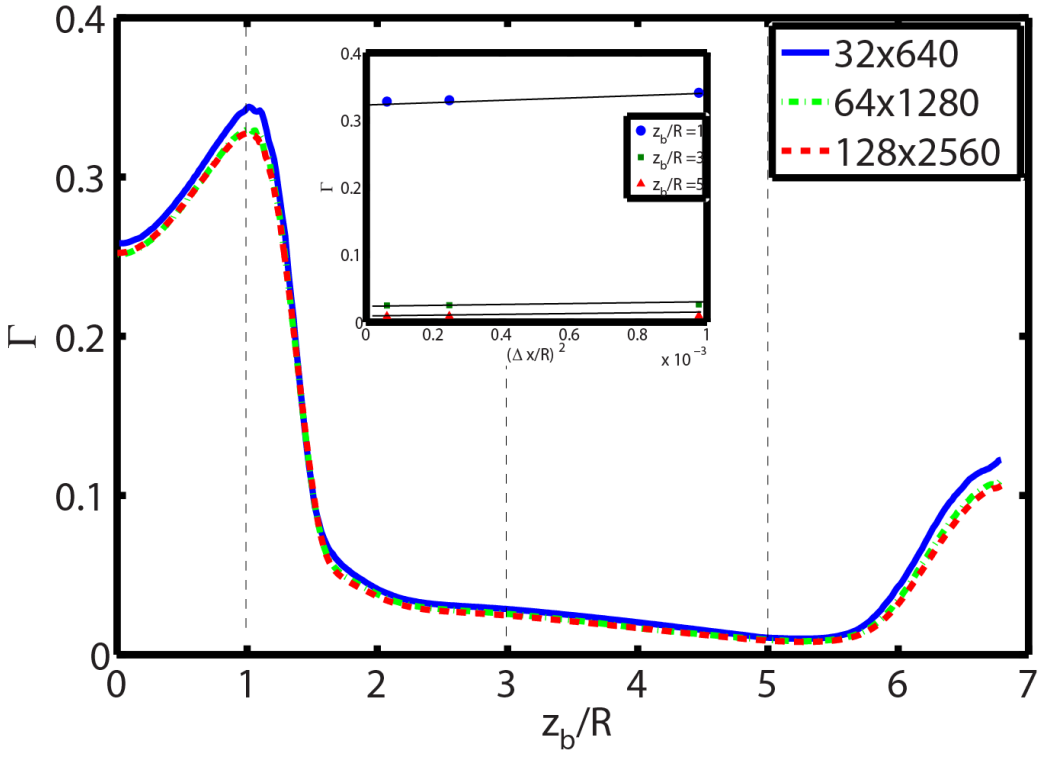

Figure 18: Grid convergence for interfacial surfactant concentration.

After that film thickness is plotted against arc length for three different grid systems and again three different locations is taken to test accuracy of the numerical scheme as can be seen in Fig 19. The grid with 32 grid cells in radial direction was sufficient to resolve all flow features and to accurately calculate film thickness within a relative error margin of 4% compared with the grid with 64 grid cells. Fig. 19 shows that film thickness is first order accurate. Therefore, we use 32 grid points in the radial direction.

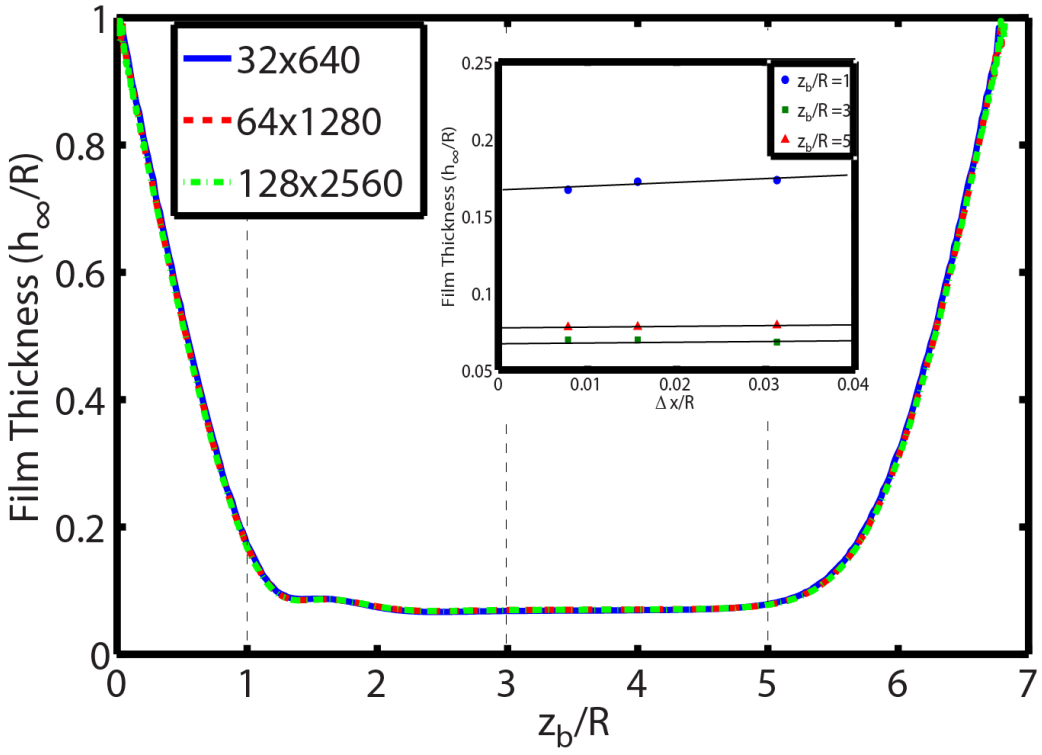

Figure 19: Grid convergence for film thickness.

BIBLIOGRAPHY

[1] Aussillous, P. and D. Quere, “Quick deposition of a fluid on the wall of a tube”. Physics of Fluids, **12(10)** 2367-2371. (2000).

[2] Krechetnikov, R. and G.M. Homsy, “Experimental study of substrate roughness and surfactant effects on the Landau-Levich law”. Physics of Fluids, **17(10)** 2005.

[3] Daripa, P. and G. Pasa, “The effect of surfactant on the motion of long bubbles in horizontal capillary tubes”. Journal of Statistical Mechanics-Theory and Experiment, 2010

[4] Bretherton, F.P., “The motion of long bubbles in tubes”. Journal of Fluid Mechanics, **10**, 166-188, (1961).

[5] Heil, M., “Finite reynolds effects in the Bretherton problem”. Physics of Fluids. **13(9)** 2517-2521, (2001).

[6] G. J. Hirasaki and J. B. Lawson, “Mechanisms of foam flow in porous media: Apparent viscosity in smooth capillaries”, SPE J. **25**, 176 (1985)

[7] Clift, R., J.R. Grace, and M.E. Weber, “Bubbles, Drops and Particles”. Dover, Mineola, (2005).

[8] Stone, H.A., “Dynamics of drop deformation and dreakup in viscous fluids”. Annual Review of Fluid Mechanics, **26**, 65-102. (1994)

[9] Grotberg, J., “Respiratory fluid mechanics and transport processes”. Annu. Rev. Biomed. Eng, **3**, 421-457, (2001).

[10] Halpern, D. et al., “Liquid and surfactant delivery into pulmonary airways”. Respiratory Physiology and Neurobiology. **163**, 222-231, (2008).

[11] Ghadiali, S.N. and D.P. Gaver, “The influence of non-equilibrium surfactant dynamics on the flow of a semi-infinite bubble in a rigid cylindrical capillary tube”. Journal of Fluid Mechanics, **478** 165-196, (2003).

[12] Krueger, M. A., and D. P.Gaver, III, “A theoretical model of pulmonary surfactant multilayer collapse under oscillating area conditions”. J. Colloid Interface Sci. **229** 353-364, (2000).

[13] Tchoreloff, P. A. et al., “A structural study of interfacial phospholipid and lung surfactant layers by transmission electron microscopy after Blodgett sampling: influence of surface pressure and temperature”. Chem. Phys. Lipids. **59** 151-165, (1991).

[14] Heil, M. et al. “Mechanics of airway closure”. Respiratory Physiology and Neurobiology. **163** 214-221, (2008).

[15] Levitzky, M. G. “Pulmonary Physiology”. McGraw-Hill. (1991).

[16] Fairbrother, F. and A.E. Stubbs, “Studies in electroendosmosis part VI. the bubble-tube methods of measurements”. Journal of Chemical Society, **1** 527-529. 1935.

[17] Taylor, G.I., “Deposition of a viscous fluid on the wall of a tube”. Journal of Fluid Mechanics, **10** 161-165. (1961).

[18] Ratulowski, J. and H. C. Chang, “Marangoni effects of trace impurities on the motion of long gas-bubbles in capillaries”. Journal of Fluid Mechanics, **210** 303-328. (1990).

[19] Stebe, K.J. and D. Barthes-Biesel, “Marangoni effects of adsorption-desorption controlled surfactants on the leading end of an infinitely long bubble in a capillary”. Journal of Fluid Mechanics, **286** 25-48. (1995).

[20] Chen, J.D., “Measuring the film thickness surrounding a bubble inside a capillary”. Journal of Colloid and Interface Science, **109(2)** 341-349. (1986).

[21] Schwartz, L.W., H.M. Princen, and A.D. Kiss, “On the motion of bubbles in capillary tubes”. Journal of Fluid Mechanics, **172** 259-275. (1986).

[22] Ginley, G.M. and C.J. Radke, “Influence of soluble surfactants on the flow of long bubbles through a cylindrical capillary”. Acs Symposium Series, **396** 480-501. (1989).

[23] Park, C.W., “Influence of soluble surfactants on the motion of a finite bubble in a capillary-tube”. Physics of Fluids a-Fluid Dynamics, **4(11)** 2335-2347. (1992).

[24] Wassmuth, F., W.G. Laidlaw, and D.A. Coombe, "Calculation of interfacial flows and surfactant redistribution as a gas-liquid interface moves between 2 parallel plates". Physics of Fluids a-Fluid Dynamics, **5(7)** 1533-1548. (1993).

[25] Severino, M., M.D. Giavedoni, and F.A. Saita, "A gas phase displacing a liquid with soluble surfactants out of a small conduit: The plane case". Physics of Fluids, **15(10)** 2961-2972. (2003).

[26] Krechetnikov, R. and G.M. Homsy, "Surfactant effects in the Landau-Levich problem". Journal of Fluid Mechanics, **559** 429-450. (2006).

[27] Muradoglu, M. and G. Tryggvason, "A front-tracking method for computation of interfacial flows with soluble surfactants". Journal of Computational Physics, **227(4)** 2238-2262. (2008).

[28] Levich, V.G., "Physicochemical Hydrodynamics". Englewood Cliffs: Prentice-Hall. (1962)

[29] Unverdi, S.O. and G. Tryggvason, "A Front-Tracking method for viscous, incompressible, multi-fluid flows". Journal of Computational Physics, **100(1)** 25-37. (1992).

[30] Harlow, F.H. and J.E. Welch, "Numerical calculation of time-dependent viscous incompressible flow of fluid with free surface". Physics of Fluids, **8** 2182-2189. (1965).

[31] Peskin, C.S., "Numerical analysis of blood flow in the heart". Journal of Computational Physics, **25(3)** 220-252. (1977).

[32] Tryggvason, G., et al., "A front-tracking method for the computations of multiphase flow". Journal of Computational Physics, **169(2)** 708-759. (2001).

[33] Adams, J. C., "Mudpack: Multigrid Fortran software for the efficient solution of linear elliptical partial differential equations", Appl. Math. Comput., **34**, 113 (1989).

[34] James, A. J. and J. Lowengrup, "A surfactant-conserving volume-of-fluid method for interfacial flows with insoluble surfactants", J. Comp. Phys., **201**, 685 (2004)

[35] Fujioka, H. and J. B. Grotberg, “The steady propagation of a surfactant-laden liquid plug in a two-dimensional channel”. Physics of Fluids. **17**, (2005).

[36] Otis, D. R. et al. “Dynamic surface tension of surfactant TA: Experiments and theory” J. Appl. Physiol. **77** 2681, (1994).

[37] Launoissurpas, M. A. et al. “Behavior of pure and mixed Dppc liposomes spread or adsorbed at the air-water interface”. Colloid Polym. Sci. **270** 901, (1992).

[38] Ghadiali, S. N. and D. P. Gaver, “An investigation of pulmonary surfactant physicochemical behavior under airway reopening conditions”. J. Appl. Physiol. 88 493, (2000).

[39] Schurch, S. et al. “A captive bubble method reproduces the in situ behavior of lung surfactant monolayers”. J. Appl. Physiol. **67** 2389, (1989).

[40] Haefeli-Bleuer B, ER. Weibel, Morphometry of the human pulmonary acinus. Anat Rec **220**: 401–414, (1988).

VITA

GOKALP GURSEL was born in Istanbul, Turkey on January 12, 1986. He received his B.Sc. degree in Mechanical Engineering from Istanbul Technical University, Istanbul, in 2009. From February 2010 to August 2011, he worked as a teaching and research assistant with full scholarship in Koc University, Turkey. He published one conference paper. He studied about effects of surfactant on the Bretherton problem. Related paper was in preparation while thesis report was being prepared.